

光学学报

基于银/高纯钢复合膜的表面等离子体共振折射率传感器

王一晴¹, 齐跃峰^{1,2*}, 曹子尧¹, 魏林特¹, 郭星辰¹, 陈斯琦¹, 刘燕燕^{1,2}

¹燕山大学信息科学与工程学院, 河北 秦皇岛 066004;

²河北省特种光纤和光纤传感器重点实验室, 河北 秦皇岛 066004

摘要 为了解决单一金属膜结构的光纤表面等离子体共振(SPR)盐度传感器结构不稳定且灵敏度较低的问题,设计了一种高灵敏度的锥形三芯光纤结构的SPR盐度传感器。以银膜为激发表面等离子体共振的金属层,在其表面涂覆高纯钢以增强其稳定性。通过Kretschmann四层结构模型对传感器进行理论分析,结果表明,在光纤锥区纤芯模和包层模之间会出现强烈的模式耦合,在覆膜区会激发明显的等离子体共振。对涂覆银膜和高纯钢膜的SPR传感器进行折射率性能测试,在1.4%~3.6%的盐度变化范围内,涂覆银膜和高纯钢膜的SPR传感器灵敏度高达4989.34 nm/RIU,对应的盐度灵敏度为9.1 nm/%,比仅涂覆银膜的SPR传感器灵敏度提高了44%。

关键词 传感器; 表面等离子体共振; 三芯光纤; 折射率传感器; 高纯钢

中图分类号 O439 文献标志码 A

DOI: 10.3788/AOS221382

1 引言

表面等离子体共振技术以其响应速度快、精度高等优点在海水盐度等折射率检测应用方面具有独特的优势。光纤表面等离子体共振传感器基于棱镜型SPR传感器的衰减全反射(ATR)理论,克服了传统SPR传感器的局限性,既拥有光纤传感器结构简单、高密度传输及耐水性的优点,又具备表面等离子体检测技术的检测范围广、方便操作和检测灵敏度高等优势,因此光纤表面等离子体共振传感器成为传感领域的研究热点之一^[1-4]。

目前,对于光纤SPR传感器的研究主要集中在提高灵敏度和环境适应性上,改变基底结构可提高传感器的灵敏度,选择合适的表面涂层可提高传感器的环境适应性^[5-6]。基于多模光纤的SPR传感器被大量研究,但该传感器灵敏度较低、稳定性较差^[7]。锥形多芯光纤可以产生比普通阶跃型多模光纤更强的模式耦合,其本征模式具有较强的场交叠,对外界折射率的变化有更强的敏感性^[8]。2013年,Bhatia等^[9]通过在金和银膜表面加硅介质层改变传感层中的电场分布,经过实验证明在传感器灵敏度有效增加的同时,硅层还能保护金属层免受氧化,提高探针的耐久性,但硅层对环境监测的测量范围影响较大。2020年,郭志勇等^[10]设

计了一种多模-单模-多模结构的光纤折射率传感器,通过在单模光纤表面涂覆二氧化钛和银复合膜进行外界溶液测量,实验发现随着环境折射率的增加,传感器品质因数不断减小,在高折射率环境下传感器的性能较低。钢是一种熔点低、抗磨损和抗氧化能力高的稀散金属,因具有对光的渗透性高、导电性强等特点,被广泛应用于宇航、无线电和新能源等领域^[11]。此外,钢还容易在金属表面形成牢固涂层,不易与碱性溶液发生反应,具有良好的抗腐蚀能力。因此,用高纯钢作为光纤SPR传感器的外层金属能对传感器起到良好的保护作用。

本文基于SPR原理和三芯光纤的强耦合特性,设计了一种基于锥形三芯光纤的银膜/高纯钢薄膜SPR传感器,通过建立Kretschmann四层结构模型对传感器结构进行优化,使其在盐度实验中能获得较高的灵敏度。结果表明,与单一银膜结构的SPR传感器相比,所提出的锥形三芯光纤银膜/高纯钢薄膜SPR传感器的灵敏度显著提高,且耐久性良好。

2 理论与仿真分析

2.1 理论分析

所提出的锥形三芯光纤银膜/高纯钢SPR传感器结构示意图如图1所示。

收稿日期: 2022-06-28; 修回日期: 2022-08-01; 录用日期: 2022-08-29; 网络首发日期: 2022-09-10

基金项目: 国家自然科学基金重点项目(61735011)、河北省科技研发重点项目(19251703D)、中央引导地方科技发展专项(19941708G)

通信作者: *yfqi@ysu.edu.cn

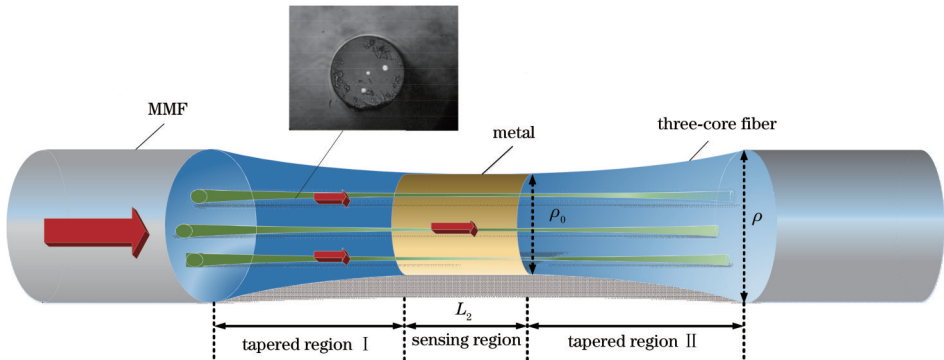


图1 三芯锥形光纤SPR传感器

Fig. 1 Three-core tapered fiber SPR sensor

三芯光纤的三个独立光波导共用一个包层,包层直径为 $125\text{ }\mu\text{m}$,中间纤芯和外侧两个纤芯直径分别为 $6\text{ }\mu\text{m}$ 和 $9.6\text{ }\mu\text{m}$,夹角为 120° 。纤芯和包层的折射率分别为1.457和1.444,中间纤芯与外侧纤芯的间距为 $35.3\text{ }\mu\text{m}$ 。

为了提高倏逝场的穿透深度,通过熔融拉锥法将三芯光纤拉制成立锥型光纤后,在锥区镀上金属膜形成传感区。三芯光纤的两端分别熔接纤芯直径为 $105\text{ }\mu\text{m}$ 的大芯径多模光纤,以保证从光源中发射出来的光能全部耦合进入三芯光纤中。第一个熔接点在纤芯和包层中充当输入或者输出耦合器。当光线进入第一个锥形过渡区域时,纤芯中的部分光会进入包层,从纤芯模式转化为包层模式,由于模式不匹配,在第二个锥形过渡区域中会产生强耦合并形成分布于数个纤芯内可以稳定传播的模式^[12]。

假设光纤的直径为 ρ ,锥腰区的直径为 ρ_0 ,传感区域的长度为 L_2 ,光以角度 θ 入射到光纤中,在锥形过渡区进行多次反射,并以角度 θ_0 耦合进锥腰区。

所设计的传感器采用在线传输式耦合结构:第一层是三芯光纤的纤芯;第二层是三芯光纤的包层,其介电常数可通过Sellmeier色散关系表示;第三层是金属层,本实验采用银作为传感层的材料;第四层是待测介质层,其折射率 n_a 在 $1.330\sim1.338$ 范围内。根据Drude公式,金属银的介电常数可以表示为

$$\epsilon_m(\lambda)=1-\frac{\lambda^2\lambda_c}{\lambda_p^2(\lambda_c+i\lambda)}, \quad (1)$$

式中: λ 为入射光波的波长; λ_p 为银的等离子体波的波长, $\lambda_p=1.4541\times10^{-7}\text{ m}$; λ_c 为金属银中电子的振荡波长, $\lambda_c=1.7614\times10^{-5}\text{ m}$ 。

高纯钢的复折射率公式^[13]可以通过波长与折射率实部和虚部变化曲线近似获得,如图2所示。

锥形光纤SPR传感器的总体反射系数可根据Kretschmann棱镜三层结构模型^[14]推导,光线在传感区的反射次数 N_{ref} 可以描述为

$$N_{\text{ref}}(\theta_0)=\frac{L_2}{2\rho_0 \tan \theta_0}, \quad (2)$$

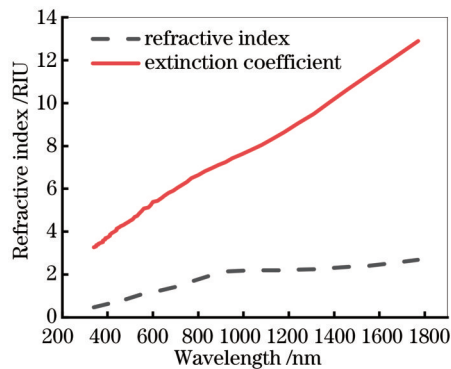


图2 高纯钢的复折射率曲线

Fig. 2 Complex refractive index curves of high-purity indium
则总的光强传输透射率^[15]可表示为

$$P(\lambda)=\frac{\int_{\theta_{0,\min}}^{\frac{\pi}{2}} [R_p(\lambda, \theta_0)]^{N_{\text{ref}}(\theta_0)} \frac{n_0^2 \sin \theta_0 \cos \theta_0}{(1-n_0^2 \cos^2 \theta_0)^2} d\theta_0}{\int_{\theta_{0,\min}}^{\frac{\pi}{2}} \frac{n_0^2 \sin \theta_0 \cos \theta_0}{(1-n_0^2 \cos^2 \theta_0)^2} d\theta_0}, \quad (3)$$

式中: R_p 表示在入射光波长为 λ 、入射角为 θ_0 时锥形光纤SPR传感器的总反射系数,可由菲涅耳公式计算; $\theta_{0,\min}$ 表示入射角的变化范围。

目前用来衡量传感器性能的参数主要有检测灵敏度和品质因数。

1)对于光纤SPR折射率传感器来说,其灵敏度可以表示为

$$S_\lambda(\lambda)=\frac{\Delta\lambda_{\text{peak}}}{\Delta n_s}, \quad (4)$$

式中: $\Delta\lambda_{\text{peak}}$ 为共振吸收峰波长位置的变化量; Δn_s 为外界环境介质折射率的变化量。当倏逝波与表面等离子体波(SPW)满足相位匹配条件时,会激发SPR效应。SPW的传播常数可以表示为

$$\beta=k_0 \sqrt{\frac{\epsilon_m n_a^2}{\epsilon_m + n_a^2}}, \quad (5)$$

式中: k_0 为光纤中传输光波数; ϵ_m 为金属膜的介电常数; n_a 为待测溶液折射率。SPW传播常数与待测溶液折射率有关,外界环境折射率发生变化,SPW的传播

常数也会发生变化,使得SPR波长发生漂移。根据SPR波长的漂移量可推得待测溶液的折射率。

2)一般用半峰全宽来表征传感器的分辨率,半峰全宽值越大,传感器分辨率越高。可以用品质因数($FOM; \eta_{FOM}$)来建立半峰全宽和灵敏度的关系^[16]。 FOM 可表示为

$$\eta_{FOM} = \frac{S \cdot D_{\text{depth}}}{\omega_{1/2}}, \quad (6)$$

式中: $\omega_{1/2}$ 为共振峰的半峰全宽; D_{depth} 为共振峰的深度。可以看出,共振峰深度与半峰全宽的比值越大, FOM 值越高,传感器的性能越好。

2.2 仿真分析

为了确定传感器的优化参数,分别对金属膜厚度、传感区长度、锥腰区直径等参数对共振吸收特性的影响进行了仿真分析。

2.2.1 金属膜厚度对共振吸收特性的影响

图3所示为银膜厚度为35~75 nm时传感器的共振光谱。可以看到,随着银膜厚度的增加,共振吸收峰的深度逐渐变浅并向长波长方向漂移。当银膜厚度在55~75 nm范围内,共振吸收峰的位置不再出现明显漂移,其深度继续变浅,这是因为倏逝波向金属膜渗透的深度有限,当金属膜厚度增加时,倏逝波激发的金属表面自由电子振荡幅度变小,入射光因激发而损耗的能量减少,共振吸收峰的深度变浅。经过计算,当金属膜厚度为45 nm时,半峰全宽较小、深度较大,传感器的品质因数较高,因此本实验选用的银膜厚度为45 nm。

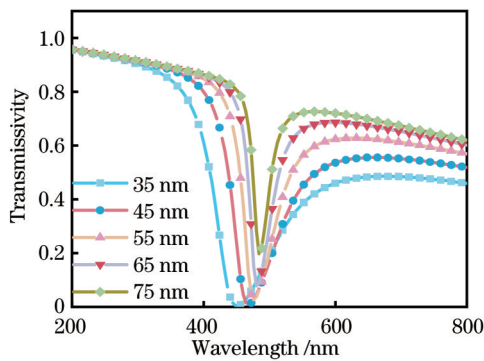


图3 不同银膜厚度下的共振光谱图

Fig. 3 Resonance spectra under different silver film thicknesses

图4所示为银膜厚度为45 nm,高纯钢膜厚度为40~60 nm时的共振光谱。随着高纯钢膜厚度的增加,共振吸收峰的深度越来越浅,半峰全宽越来越小,这是因为钢膜的增加,使表面等离子体振荡中的阻尼增大,共振吸收峰深度变浅。当高纯钢膜厚度选为45 nm时,共振峰的深度与半峰全宽的比值最大,传感器的性能最好。

2.2.2 传感区长度对共振吸收特性的影响

传感区的长度影响光波在金属覆盖区的反射次

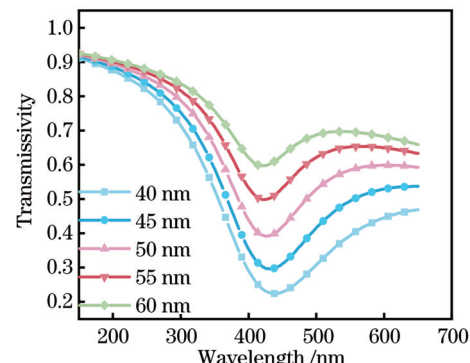


图4 银膜/高纯钢膜共振光谱图

Fig. 4 Resonance spectra of silver/high-purity indium films

数,在银膜厚度为45 nm的条件下,分别计算传感区的银膜长度为5~30 mm时传感器的光强透射率,共振光谱如图5(a)所示。随着传感区长度的增加,共振吸收峰的位置基本保持不变,深度逐渐变深,半峰全宽也逐渐变大。分析出现此种现象的原因是传感区越长,光的反射次数越多,光波每发生一次SPR现象,就会损耗掉一些能量,多次SPR效应的发生导致金属膜对光波的共振衰减叠加,导致共振深度越来越深。考虑到较浅的共振峰深度在实际测试时不易观察出,且经计算发现长度为10 mm时传感器的品质因数值较大,因此本实验选择的传感区长度为10 mm。

2.2.3 锥腰区直径对共振吸收特性的影响

图5(b)所示为锥腰区直径对共振光谱的影响。随着锥腰区直径的增大,共振峰深度越来越浅,但其位置基本不变。这是因为随着直径越来越小,光反射次数越来越多,共振区域增大,导致共振深度越来越深。同时倏逝波的穿透深度越来越大,倏逝场得到了增强,传感器的灵敏度越来越高,相应地,光在过渡区传输时的损耗也越来越大,因此光纤的直径不能过小。当锥腰区直径为45 μm时,共振峰的深度与半峰全宽的比值最大,因此实验制备传感区的直径为45 μm。

3 实验结果与讨论

考虑到所制备的光纤直径较细,使用氢气火焰拉锥法^[17]制备锥形光纤。实验对膜层平整度和黏附性有极高的要求,采用磁控溅射法^[18]对Ag膜进行镀制。由于高纯钢呈丝状,且熔点较低,采用真空热蒸发法进行制备。首先,在对三芯光纤的中间部位去除约2 cm的涂覆层后,将其放置在拉锥机的光纤夹具处,在氢气流量为156 mL/min、拉伸速度为1.4 mm/s的参数下对其进行拉锥处理。图6为拉锥后的三芯光纤实物图。将拉锥好的光纤放在磁控溅射设备真空室内进行银膜溅射,银膜的厚度为45 nm。溅射完成后将涂覆银膜的光纤放在蒸发腔内进行高纯钢膜制备。图7为镀膜后的光纤实物图。将镀膜完成后的三芯光纤与纤芯直径为105 μm、长度为2 mm的多模光纤熔接,随后在其

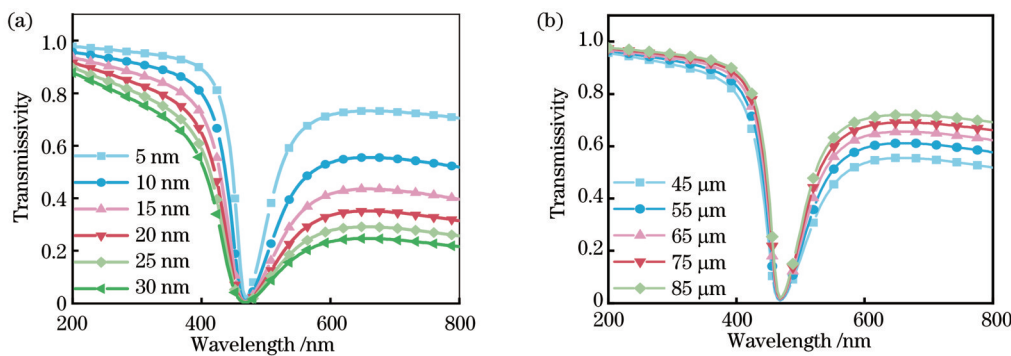


图5 不同结构参数下的共振光谱图。(a)不同传感区长度下的共振光谱;(b)不同锥腰区直径下的共振光谱

Fig. 5 Resonance spectra under different structural parameters. (a) Resonance spectra under different sensing area lengths; (b) resonance spectra under different cone waist diameters

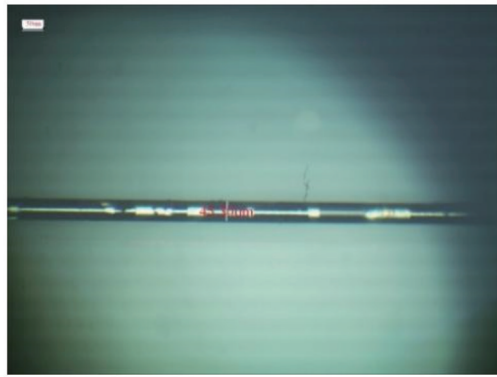


图6 锥形三芯光纤实物图

Fig. 6 Physical drawing of tapered three-core optical fiber

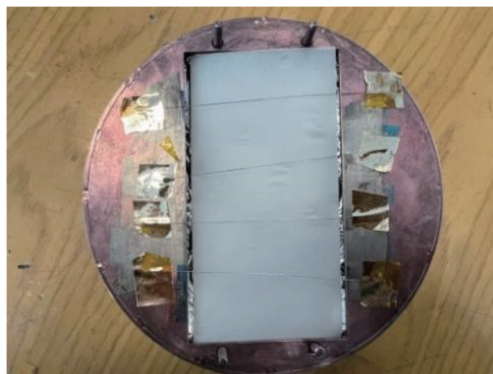


图7 镀膜光纤实物图

Fig. 7 Physical drawing of coated optical fiber

两端再熔接纤芯直径为 $62.5\text{ }\mu\text{m}$ 的多模光纤用于连接光源和光谱仪。

配置溶液质量分数变化范围为 $1\% \sim 3.6\%$ 的盐溶液,用阿贝折射仪测量得到其对应折射率范围为 $1.33 \sim 1.338$,将溶液质量分数与其对应的折射率绘制关系曲线,得到

$$y = 0.00183x + 1.3316, \quad (7)$$

式中: y 表示溶液的折射率; x 表示溶液的质量分数。

实验系统示意图如图8所示,AvaLight-HAL型卤素灯光源中发出的光经过传感器,由AvaSpec-2048-

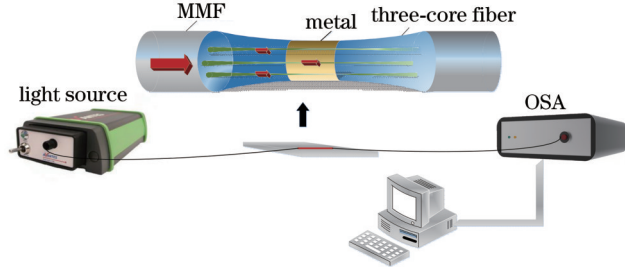


图8 折射率传感测量实验装置示意图

Fig. 8 Schematic of refractive index sensing and measuring experimental device

USB2型光纤光谱仪采集光学信号。

1) 仅涂覆单一银膜的传感器

仅涂覆单一银膜的SPR传感器透射光谱和共振波长与溶液折射率的变化关系分别如图9(a)、(b)所示。可以看到,随着溶液折射率的增加,传感器的共振吸收峰向长波长方向漂移且共振深度逐渐增加。从图9(b)所示的拟合结果看到,当溶液折射率从 1.335 变化到 1.338 ,所设计的基于单一银膜的三芯锥形光纤SPR传感器的灵敏度达到 3450.74 nm/RIU ,根据式(7)转化得到的质量分数灵敏度为 $5.7\text{ nm}/\%$ 。盐溶液与SPR共振波长的线性关系良好,拟合系数为 0.978 。

2) 涂覆银/高纯铜的SPR传感器

利用镀有 45 nm 银膜和 45 nm 高纯铜膜的SPR传感器测得的共振光谱和拟合曲线如图10(a)、(b)所示。从图10(a)可看到,在 $1.334 \sim 1.338$ 的折射率范围内,共振吸收峰随着盐溶液折射率的增大而向长波长方向发生明显漂移。共振峰的位置与仅涂覆银膜的SPR传感器相比,整体向长波长方向偏移。这是因为加入高纯铜薄膜后,其介电常数的实部影响着共振峰的位置。图10(b)中,共振波长与溶液折射率的拟合度 R^2 为 0.994 ,共振波长随着溶液折射率的变化呈现较好的线性关系。传感器灵敏度为 4989.34 nm/RIU ,其质量分数灵敏度为 $9.1\text{ nm}/\%$ 。涂覆银/高纯铜的SPR传感器能获得十万分之一质

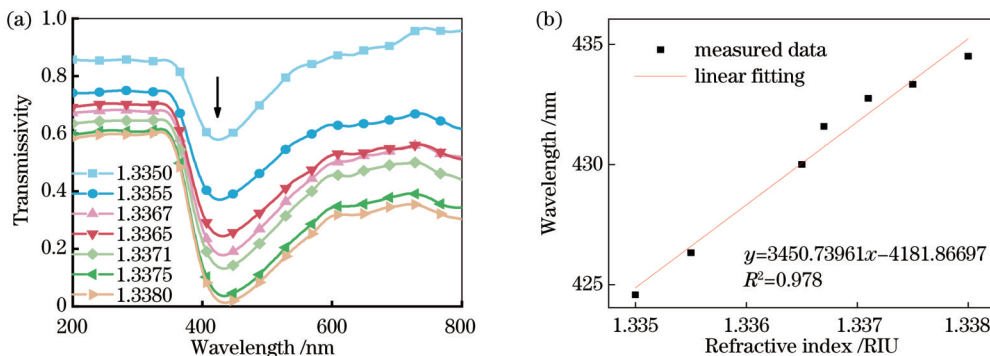


图9 镀银膜SPR传感器透射光谱和共振波长与折射率拟合结果。(a)归一化透射光谱;(b)共振波长与溶液折射率拟合结果

Fig. 9 Transmission spectra and fitting results of resonance wavelength and refractive index of silver plated SPR sensor.

(a) Normalized transmission spectra; (b) fitting results of resonance wavelength and refractive index of solution

量分数的分辨率,比仅涂覆银膜的光纤SPR传感器的灵敏度提高约44%。这是因为铟有较高的介电常数^[19],高折射率材料的存在能增加倏逝波的穿透深度^[20],倏逝场增强,导致倏逝波与SPW波的相互作用

增强,银膜的等离子体效应增强,引起波长漂移增大,进而提高传感器的灵敏度。与文献[21]的传统光纤SPR传感器相比,涂覆银/高纯铟的SPR传感器灵敏度提高了126%左右。

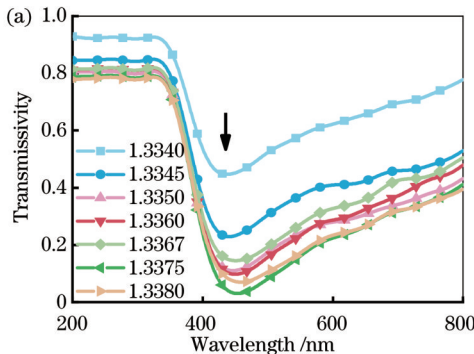


图10 涂覆银/高纯铟的SPR传感器的透射光谱和共振波长与溶液折射率的拟合结果。(a)归一化透射光谱;(b)共振波长与溶液折射率拟合曲线

Fig. 10 Transmission spectra and fitting results of resonance wavelength and refractive index of SPR sensor with high-purity indium and silver film. (a) Normalized transmission spectra; (b) fitting results of resonance wavelength and refractive index of solution

国家海洋科学数据中心的统计数据显示,从海水表面至-5000 m的海深内,海水的盐度范围变化为2%~3.5%,而所设计传感器的质量分数测量范围为1.4%~3.6%,能实现0~-5000 m深度范围内的海

水盐度测量。

将提出的传感器与其他已报道的SPR传感器进行比较,结果如表1所示。可以看出,所设计的传感器灵敏度有显著提升且稳定性良好。

表1 不同结构传感器的比较
Table 1 Comparison of sensors with different structures

Fiber type	Sensor structure	Refractive index range	Sensitivity / (nm·RIU ⁻¹)	Ref.
Multimode fiber	Au	1.3335~1.4018	2207.33	[21]
Singlemode fiber	Au	1.3364~1.4279	3582.00	[22]
Multimode fiber	Au Taper fiber	1.3353~1.3453	1914.00	[23]
Plastic optical fiber	Au-Ag-MoS ₂	1.3330~1.4330	3061.00	[24]
Plastic optical fiber	Graphene-Au	1.3330~1.3394	6500.00	[25]
Prism	Au-WS ₂	1.3330~1.3360	2459.30	[26]
Three-core optical fiber	Ag/In	1.3350~1.3380	4989.34	Proposed

4 结论

设计了一种基于锥形三芯光纤的Ag/In结构SPR

传感器。传感器基于三芯光纤的强耦合特性和倏逝场激发特性进行传感,通过实验探究了高纯铟对光纤SPR传感器的影响。采用磁控溅射技术和热蒸发镀

膜法分别镀制银膜和高纯铜膜,实验结果表明基于Ag/In的SPR传感器在1.4%~3.6%的质量分数测量范围内,其折射率灵敏度提高44%左右,可实现0~5000 m范围的海水盐度测量。由此可见,在银膜外引入高纯铜能提高传感器的灵敏度和稳定性,该传感器在环境监测、生物分子测量和气候预测等领域具有较高的应用潜力。

参考文献

- [1] Liu Y C, Chen H L, Li S G, et al. Surface plasmon resonance-induced tunable polarization filters based on nanoscale gold film-coated photonic crystal fibers[J]. Chinese Physics B, 2017, 26(10): 275-279.
- [2] 马金英, 刘铁根, 江俊峰, 等. 光纤表面等离子体共振传感灵敏度提高研究进展[J]. 中国激光, 2021, 48(19): 1906002. Ma J Y, Liu T G, Jiang J F, et al. Progress in sensitivity enhancement for optical fibre surface plasmon resonance sensing [J]. Chinese Journal of Lasers, 2021, 48(19): 1906002.
- [3] 范雨艳, 施伟华. 基于表面等离子体共振的光子晶体光纤生物传感[J]. 激光与光电子学进展, 2021, 58(21): 2106003. Fan Y Y, Shi W H. Photonic crystal fiber biosensors based on surface plasmon resonance[J]. Laser & Optoelectronics Progress, 2021, 58(21): 2106003.
- [4] 王双双, 黄勇林, 詹平. 基于正十六边形光子晶体光纤的表面等离子体共振传感器[J]. 激光与光电子学进展, 2022, 59(7): 0706001. Wang S S, Huang Y L, Zhan P. Surface plasmon resonance sensor based on photonic crystal fiber in regular Hexadecagon[J]. Laser & Optoelectronics Progress, 2022, 59(7): 0706001.
- [5] 宋晓, 赵雪薇, 洪瑞金, 等. Al/Al₂O₃复合薄膜的制备及表面等离子体共振性能研究[J]. 光学学报, 2015, 35(12): 1231001. Song X, Zhao X W, Hong R J, et al. Fabrication and the surface plasmon resonance properties of Al/Al₂O₃ composite films[J]. Acta Optica Sinica, 2015, 35(12): 1231001.
- [6] Lou J B, Cheng T L, Li S G, et al. Surface plasmon resonance photonic crystal fiber biosensor based on gold-graphene layers[J]. Optical Fiber Technology, 2019, 50: 206-211.
- [7] Wu L, Chu H S, Koh W S, et al. Highly sensitive graphene biosensors based on surface plasmon resonance[J]. Optics Express, 2010, 18(14): 14395-14400.
- [8] Wang F, Wang R F, Wang X, et al. Three-core fiber cascade asymmetric dual-taper robust structure for the simultaneous measurement of a mass concentration of a glucose solution and temperature[J]. Optics Communications, 2020, 461: 125227.
- [9] Bhatia P, Gupta B D. Surface plasmon resonance based fiber optic refractive index sensor utilizing silicon layer: effect of doping[J]. Optics Communications, 2013, 286: 171-175.
- [10] 郭志勇, 葛益娴, 沈令闻, 等. 基于MSM结构的表面等离子体共振光纤折射率传感器[J]. 半导体光电, 2020, 41(2): 205-210. Guo Z Y, Ge Y X, Shen L W, et al. Surface plasmon resonance fiber refractive index sensor based on MSM structure[J]. Semiconductor Optoelectronics, 2020, 41(2): 205-210.
- [11] 韩汉民. 高纯钢的制备[J]. 化学世界, 1995, 36(4): 174-177. Han H M. Preparation of high purity indium[J]. Chemical World, 1995, 36(4): 174-177.
- [12] An G W, Li S G, Yan X, et al. High-sensitivity and tunable refractive index sensor based on dual-core photonic crystal fiber [J]. Journal of the Optical Society of America B, 2016, 33(7): 1330-1334.
- [13] Mathewson A G, Myers H P. Absolute values of the optical constants of some pure metals[J]. Physica Scripta, 1971, 4(6): 291-292.
- [14] Kretschmann E, Raether H. Radiative decay of non radiative surface plasmons excited by light[J]. Zeitschrift Für Naturforschung A, 1968, 23(12): 2135-2136.
- [15] Ankiewicz A, Pask C, Snyder A W. Slowly varying optical fibers[J]. Journal of the Optical Society of America, 1982, 72(2): 198-203.
- [16] 林华, 张娟, 朱晓松, 等. 基于金属-介质-金属多层膜结构的空芯光纤折射率传感器[J]. 光学学报, 2018, 38(6): 0606006. Lin H, Zhang X, Zhu X S, et al. Refractive index sensor based on hollow optical fiber with metal-dielectric-metal multilayered films structure[J]. Acta Optica Sinica, 2018, 38(6): 0606006.
- [17] 孙伟民, 石帅, 戴强. 拉锥光纤的制作工艺与测试方法[J]. 光电子·激光, 2009, 20(11): 1474-1477. Sun W M, Shi S, Dai Q. Fabrication and measurement of tapered fibers[J]. Journal of Optoelectronics·Laser, 2009, 20(11): 1474-1477.
- [18] Xu Z, Yu X Z, Shen Z G. Coating metals on micropowders by magnetron sputtering[J]. China Particuology, 2007, 5(5): 345-350.
- [19] Zhang J B, Zheng Y X, Wang Z Y, et al. Structural characterization, optical properties, and phase transitions of In_{1-x}Sn_x alloy thin films[J]. The Journal of Physical Chemistry C, 2016, 120(14): 7822-7828.
- [20] Lahav A, Auslender M, Abdulhalim I. Sensitivity enhancement of guided-wave surface-plasmon resonance sensors[J]. Optics Letters, 2008, 33(21): 2539-2541.
- [21] Kanso M, Cuenot S, Louarn G. Sensitivity of optical fiber sensor based on surface plasmon resonance: modeling and experiments[J]. Plasmonics, 2008, 3(2): 49-57.
- [22] 朱彩莲, 吴乐南, 杨洋. 光纤表面等离子体波传感器测量液体折射率的研究[J]. 传感技术学报, 2004, 17(4): 675-678. Zhu C L, Wu L N, Yang Y. Research on liquid refractive index measured by the optic-fiber surface plasmon wave sensor[J]. Chinese Journal of Sensors and Actuators, 2004, 17(4): 675-678.
- [23] Al-Qazwini Y, Noor A S M, Yaacob M H, et al. Experimental realization and performance evaluation of refractive index SPR sensor based on unmasked short tapered multimode-fiber operating in aqueous environments[J]. Sensors and Actuators A, 2015, 236: 38-43.
- [24] Wang Q, Jiang X, Niu L Y, et al. Enhanced sensitivity of bimetallic optical fiber SPR sensor based on MoS₂ nanosheets[J]. Optics and Lasers in Engineering, 2020, 128: 105997.
- [25] Wei W, Nong J P, Zhu Y, et al. Graphene/Au-enhanced plastic clad silica fiber optic surface plasmon resonance sensor[J]. Plasmonics, 2018, 13(2): 483-491.
- [26] Wang H, Zhang H, Dong J L, et al. Sensitivity-enhanced surface plasmon resonance sensor utilizing a tungsten disulfide (WS₂) nanosheets overlayer[J]. Photonics Research, 2018, 6(6): 485-491.

Surface Plasmon Resonance Refractive Index Sensor Based on Silver/ High-Purity Indium Composite Film

Wang Yiqing¹, Qi Yuefeng^{1,2*}, Cao Ziyao¹, Wei Linte¹, Guo Xingchen¹, Chen Siqui¹,
Liu Yanyan^{1,2}

¹School of Information Science and Engineering, Yanshan University, Qinhuangdao 066004, Hebei, China;

²Key Laboratory for Special Fiber and Fiber Sensor of Hebei Province, Qinhuangdao 066004, Hebei, China

Abstract

Objective As people tend to pay much attention to the ecological environment, the detection of liquid salinity in hydrological environments has gradually become an indispensable part of research fields such as agricultural planting, aquaculture, and monitoring of the marine environment. Surface plasmon resonance (SPR) technology has unique advantages in liquid salinity detection due to its fast response speed and high precision. The optical fiber SPR sensor combines optical fiber and plasma technology to overcome the limitations of prism-type SPR sensors. It not only has the advantages of simple structure and water resistance of optical fiber sensors but also has a wide detection range and high detection sensitivity of surface plasmon technology and convenient operation. However, traditional optical fiber SPR sensors based on multi-mode or single-mode single metal film structures generally face many problems. Specifically, the metal film is easy to fall off, and the detection sensitivity is low. In addition, the stability is poor. Indium has excellent electrical properties and positive flexibility. Therefore, it is an important optoelectronic material and is easy to form a firm coated on a metal surface. Furthermore, it is not easy to react with alkaline solutions and has good corrosion resistance. Therefore, this paper uses the strong coupling characteristics of a three-core fiber and the principle of SPR to design a tapered fiber SPR sensor based on a silver film and a high-purity indium film, which can improve the sensitivity and corrosion resistance of the sensor.

Methods This thesis is based on the theory of an optical fiber SPR sensor, and the propagation law of light in a tapered fiber is studied. The total reflection coefficient of the sensor is obtained by using the Fresnel formula, and the influence of the diameter of the cone waist region, the length of the sensing region, and the thickness of the metal film on the sensor is analyzed by numerical calculation, and the optimal parameters are determined. The sensor is fabricated according to the numerical values determined by the simulation, and the optical fiber is tapered by a hydrogen flame fusion taper. The silver film and the high-purity indium film are prepared by magnetron sputtering and molecular vapor deposition, respectively. First, the optical fiber SPR sensor with a single silver film structure is studied, and the change in its resonance peak is observed by dropping salt solutions of different mass fractions. Then, under the same experimental conditions, the sensing performance of the optical fiber SPR sensor with silver film and high-purity indium film structures is studied. After comparing the two sets of experimental data, a conclusion is drawn.

Results and Discussions The designed fiber SPR sensor with silver film and high-purity indium film structures has an excellent performance in salinity detection. Fig. 8 shows the resonance spectrum of the structure coated with only a single silver film. As the refractive index of the external environment increases, the resonance peak shifts to the long wavelength direction, and the sensor shows a small amount of wavelength shift. After calculation, the SPR sensor with a single silver film structure has a refractive index sensitivity of 3450.74 nm/RIU. For the SPR sensor with a silver film structure in Fig. 9, its resonance peak shifts significantly to the long wavelength direction as the refractive index of the solution increases. The linear relationship between the resonance wavelength and the refractive index of the solution is positive, and the sensitivity of the sensor is as high as 4989.34 nm/RIU, which is converted into a mass fraction sensitivity of 9.1 nm/% by Eq. 7. This is because high-purity indium has a higher refractive index, and the presence of high-refractive-index materials can increase the penetration depth of evanescent waves, and the evanescent field is enhanced, which results in an increase in the interaction between evanescent waves and surface plasmon waves. The plasmonic effect of the silver film is enhanced, which in turn causes an increase in wavelength drift and improves the sensitivity of the sensor. Compared with that of the SPR sensor coated with only a single silver film structure, the sensitivity is improved by about 44%. Compared with that of the traditional fiber SPR sensor, the sensitivity is improved by about 126%.

Conclusions In this paper, an Ag/In structure SPR sensor based on a three-core fiber is designed. The multi-core fiber SPR sensing mechanism is theoretically analyzed, and the system structure parameters are determined. In addition, two fiber SPR sensors with only a single silver film structure and a silver film plus high-purity indium structure are

experimentally studied. By comparing the experimental results, the resonance peak of the Ag/In structure SPR sensor shows a larger wavelength shift, and its refractive index sensitivity is about 44% higher than that of the Ag structure fiber SPR sensor in a mass fraction measurement range of 1.4%-3.6%, which can realize salinity measurement in a full depth range of 0—5000 m. Therefore, the introduction of high-purity indium outside the silver film can improve the sensitivity and stability of the sensor, and the sensor can be applied in fields such as environmental monitoring, biomolecular measurement, and climate prediction.

Key words sensors; surface plasmon resonance; three-core fiber; refractive index sensors; high-purity indium